Uniformity of Laser-Induced Periodic Surface Structures and Their Effect on the Antibacterial Performance of Stainless Steel

Mikuru Okazaki[*1], Masaki Hashida[2,3], and Satoru Iwamori[1]

[1]*Course of Science and Technology, Tokai University, 4-1-1 Katakana, Hiratsuka, Kanagawa 259-1292, Japan*
[2]*Research Institute of Science and Technology, Tokai University, 4-1-1 Kitakaname, Hiratsuka, Kanagawa 259-1292, Japan*
[3]*Institute for Chemical Research, Kyoto University, Gokasho, Uji, Kyoto, 611-0011, Japan*
[*]*Corresponding author's e-mail: 3mtad003@tokai.ac.jp*

To evaluate the antibacterial performance of laser-induced periodic surface structures (LIPSS) formed on SUS430 stainless steel (equivalent to AISI 430, ferritic stainless steel), surface patterns were fabricated using femtosecond laser pulses (wavelength: 1030 nm; pulse duration: 150 fs) with controlled fluence. Two types of LIPSS were produced with average ridge and valley widths of approximately 410-nm and 380-nm/750-nm mixed structure, respectively. Antibacterial performance was assessed against *Escherichia coli* using the film-attachment method in accordance with the JIS Z 2801:2021 standard. Compared with the untreated SUS430 surface, the 410-nm LIPSS surface exhibited a reduction of approximately 83% in bacterial colony count, while the 380-nm/750-nm mixed structure showed a reduction of only about 31%. Fast Fourier transform analysis of scanning electron microscopy images revealed that the 410-nm structures had finer ridge and valley widths and higher structural uniformity. These findings suggest that the geometric characteristics of LIPSS, particularly ridge and valley width and uniformity, play a crucial role in enhancing antibacterial performance. This study demonstrates the potential of femtosecond laser processing as a novel approach to impart antibacterial functionality to material surfaces without the use of chemical agents.
DOI: 10.2961/ilmn.2026.01.2003
Keywords: femtosecond laser, stainless steel, LIPSS, antibacterial performance

1. Introduction

The excessive and inappropriate use of antibiotics has led to a global increase in antimicrobial-resistant bacteria [1], posing a serious public health threat. Conventional chemical-based antibacterial strategies face significant limitations due to the emergence of resistance and environmental concerns, thereby driving interest in alternative approaches that do not rely on chemical agents. Among these, surface modification using micro- and nanoscale structures has emerged as a promising strategy to impart antibacterial performance through purely physical means [2,3]. In addition to their antibacterial performance, such structures are known to exhibit various functionalities depending on their geometric scale, including control of wettability, friction, and reflectivity [4-7].

Laser processing is a flexible and simple technique that enables the modification of various materials without the use of chemical agents. Laser-induced periodic surface structures (LIPSS) [8-10] are periodic surface morphologies formed by ultrafast laser irradiation, where parameters such as fluence and wavelength can be adjusted to control features such as ridge and valley width and periodicity. While the antibacterial performance of LIPSS has been reported [11,12], the influence of their structural characteristics—particularly ridge and valley width and structural uniformity—on antibacterial performance has not yet been fully elucidated.

In this study, we systematically investigated LIPSS formed on SUS430 stainless steel surfaces using femtosecond laser pulses and evaluated their antibacterial performance against *Escherichia coli*, aiming to elucidate the relationship between structural characteristics and antibacterial performance.

2. Materials and methods

2.1 Ablation threshold measurement and LIPSS fabrication

The formation of LIPSS on metal surfaces using pulsed lasers is known to occur near the ablation threshold fluence, and it has been reported that the structural characteristics change depending on the laser fluence [13]. Therefore, prior to evaluating the LIPSS structures, the ablation threshold of SUS430 was measured. A schematic of the optical setup is shown in Fig. 1.

A femtosecond laser (CARBIDE CB-5SP, Light Conversion; wavelength: 1030 nm; pulse duration: 150 fs; repetition rate: 0.5 kHz) was used to irradiate the mirror-polished surface of SUS430 substrates (25 mm × 25 mm; thickness:

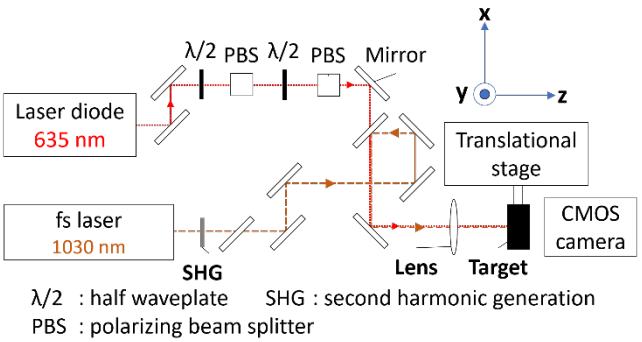

Fig 1 Schematic diagram of the optical setup for laser irradiation.

1 mm). The laser beam was monitored using a CMOS camera and focused on a spot diameter of approximately 45 μm with a plano-convex lens of 100-mm focal length, resulting in a Gaussian spatial profile.

The fluence was varied from 0.20 J/cm² to 1.20 J/cm², and the crater diameter (with laser ablation) was measured after 50-100 pulses using a laser scanning microscope (LEXT4500, OLYMPUS Co., Ltd.). A laser diode (wavelength: 635 nm) was used to trace the optical path of the femtosecond laser and to assist in aligning the irradiation position. The SUS430 surface before laser irradiation was measured using the laser scanning microscope.

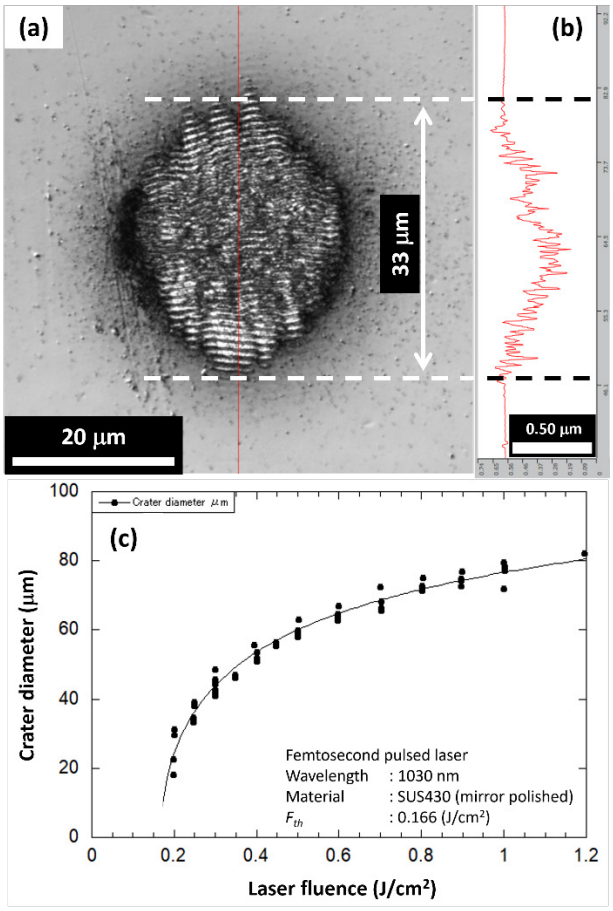

Fig 2 (a) Laser scanning microscope image of crater produced on SUS430 surface with laser ablation. (b) Cross-sectional view of (a). (c) Dependence of crater diameter on laser fluence.

The surface was mirror-polished, resulting in an arithmetic mean height (Sa) of approximately 2 nm, and it was fixed on a linear translation stage. The scan speed of the translation stage in the horizontal direction was adjusted to control the average number of pulses per spot.

Figure 2(a) shows the 3D profile of a crater produced by laser irradiation with a laser fluence of 0.25 J/cm² and 50 pulses. Figure 2(b) shows a cross-sectional view of the crater at its deepest position as shown by the red line in Fig. 2(a). The crater diameter was 33 μm, which was defined by the falling edges in Fig. 2(b). Figure 2(c) summarizes the experimentally observed crater diameters (solid circles) as a function of laser fluence; the curve is a least-squares fit of those diameters. To evaluate the ablation threshold [14,15], the fitting was applied using a Gaussian spatial profile of the laser spot on the SUS430 surface, and extrapolating the fitted curve, the ablation threshold of the mirror-polished SUS430 was determined to be 0.166 J/cm². The values of laser fluence reported in this study refer to the peak fluence per pulse [16,17].

For LIPSS fabrication on a 25 mm × 25 mm SUS430 substrate, laser pulses with a 5-kHz repetition rate were irradiated at a fluence of 0.20–0.40 J/cm², close to the ablation threshold. To fabricate the LIPSS entirely, the translation stage moved the SUS430 along the X-axis for 100 pulses, and the hatching distance was 50 μm along the Y-axis (see Fig. 1). The hatching distance was a little wider than the laser spot diameter of 45 μm. The maximum applied fluence was limited to 0.40 J/cm² because any higher would have destroyed the LIPSS.

2.2 Surface characterization

The surface morphology was observed using a field-emission scanning electron microscope (FE-SEM; JSM-7100F, JEOL Ltd.). FE-SEM images were acquired at an accelerating voltage of 15.0 kV and a working distance of 41.1 mm under high-vacuum conditions (9.6×10^{-5} Pa). Fast Fourier transform (FFT) analysis was performed on 10 randomly selected regions from the SEM images, and the averaged results were used to evaluate the periodicity and uniformity based on the perpendicular period and phase scanning (P^3S) method [18]. The periodicity of the LIPSS was the FFT peak in spatial frequency, and its uniformity Δω was defined as the full width at half maximum (FWHM) at the peak of the FFT spectrum.

2.3 Characterization of antibacterial properties

Antibacterial performance was evaluated using the film-attachment method in accordance with the JIS Z 2801:2021 standard. *E. coli* (DH5α) was used as the test strain and incubated at 35 ± 1 °C. All instruments used in the experiment were sterilized by autoclaving, and to prevent contamination of the sample surfaces, ultrasonic cleaning was performed in ethanol and ultrapure water, followed by drying in a thermostatic chamber at 35 ± 1 °C. Luria–Bertani (LB) broth (Difco™, LB Broth, Miller, BD) and standard agar medium (ATECT, standard ager) were used as the liquid and solid culture media, respectively.

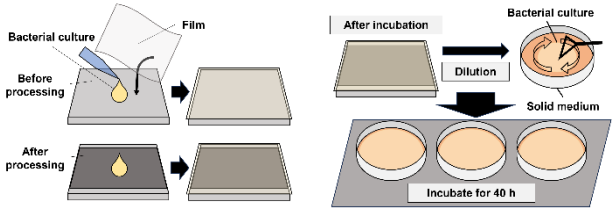

Fig. 3 Schematic of antibacterial evaluation procedure using film-attachment method (steps 2–4).

The experiment involved the following four steps:
(Step 1) preparation of the liquid culture medium and incubation of *E. coli*,
(Step 2) adjustment of bacterial concentration using McFarland turbidimetry and film attachment,
(Step 3) removal of the film, dilution of the bacterial suspension, and cultivation for 40 h on solid media,
(Step 4) colony counting to evaluate the bacterial reduction rate.

Figure 3 shows a schematic illustration of the antibacterial evaluation. The antibacterial effect was assessed based on the reduction rate of colony numbers on the LIPSS-treated surfaces compared with the untreated surfaces. In the procedure, 400 µL of liquid culture medium was dropped onto the 25 mm × 25 mm square samples, resulting in an estimated thickness of approximately 640 µm. Since the medium remained static during the test and the bacteria tended to settle, sufficient contact with the structured surface is considered to have been maintained throughout the incubation.

3. Results and discussion

3.1 Surface morphology and structural analysis

Figure 4 shows SEM images of LIPSS formed on SUS430 surfaces by femtosecond laser irradiation at fluences of 0.20 J/cm² and 0.30–0.40 J/cm². For metals, the periodicity of LIPSS depending on laser fluence has been reported [19-21], and the tendency is similar for SUS430. The LIPSS fabricated at 0.20 J/cm² exhibited a single distinct periodic structure with an average ridge and valley width of approximately 410 nm and a Δω value of 0.37, indicating high uniformity. The depth was measured using an atomic force microscope (LEXT4500, OLYMPUS Co., Ltd.) and was found to be approximately 120 nm. It has been reported that an appropriate LIPSS depth can suppress bacterial adhesion and considerably influence antibacterial performance [22]. In contrast, the LIPSS produced at 0.30–0.40 J/cm² exhibited two distinct peaks in the frequency domain, suggesting that the primary structure, with a ridge and valley width of 380 nm, was mixed with an additional component around 750 nm.

The uniformity and periodicity of these structures were evaluated using FFT analysis based on the P^{3}S method, as shown in Fig. 5. A smaller Δω value obtained from the FWHM of the FFT peak indicates higher structural uniformity. The Δω values for these structures ranged from 0.37 to 0.81, indicating lower structural uniformity compared with those formed at 0.20 J/cm². These results indicate that narrower ridge and valley widths and higher structural uniformity contribute considerably to the inhibition of bacterial adhesion.

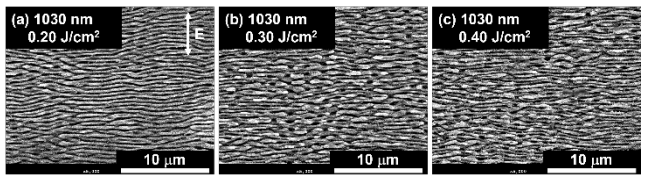

Fig. 4 FE-SEM images (×5000 magnification) of LIPSS formed on SUS430 surface by laser irradiation.

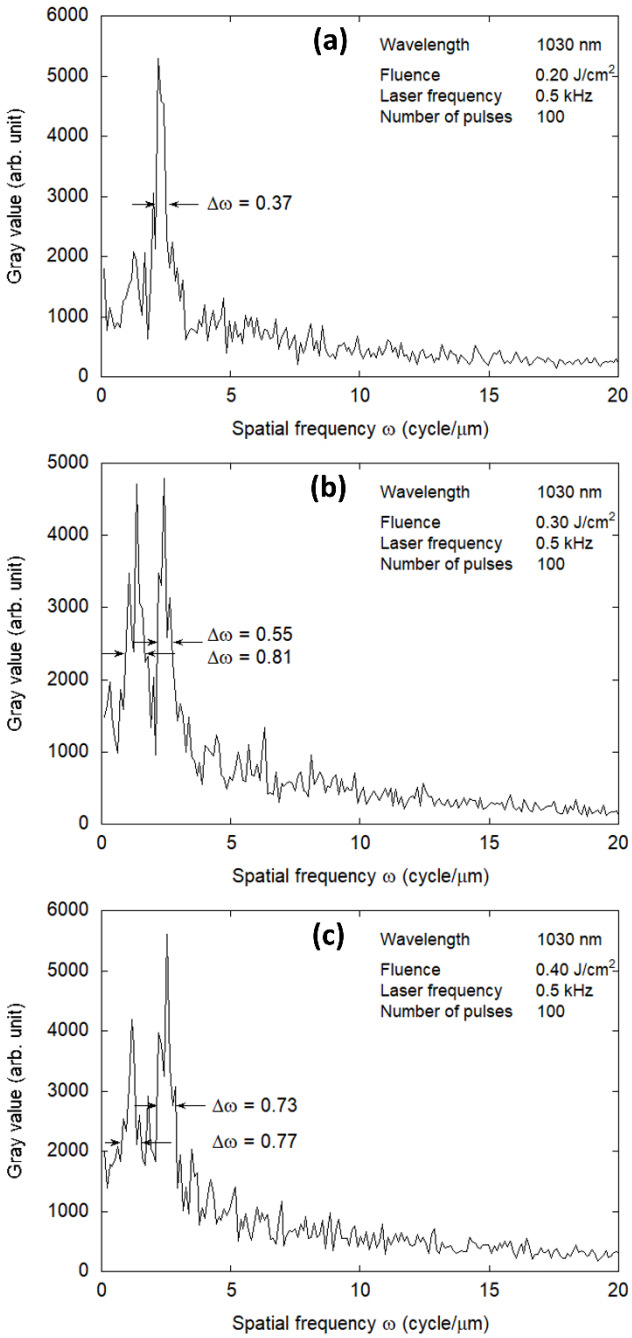

Fig. 5 Evaluation results for periodicity and uniformity of LIPSS analyzed by FFT based on P^{3}S method: (a) 0.20 J/cm² (Δω = 0.37); (b) 0.30 J/cm² (Δω = 0.55-0.81); (c) 0.40 J/cm² (Δω = 0.73-0.77).

3.2 Antibacterial performance

The antibacterial performance of the LIPSS-treated surfaces was evaluated using the film-attachment method with *E. coli*. The antibacterial tests were performed in triplicate ($n = 3$) for every condition. Figure 6 shows images of colonies on solid media after 40 h of incubation. The number of active colonies is summarized below as the mean ± standard deviation. For untreated SUS430, there were 1181 ± 94 colonies; for 410-nm LIPSS at 0.20 J/cm^2, there were 204 ± 56 colonies; and for 380-nm/750-nm mixed LIPSS at 0.30–0.40 J/cm^2, there were 813 ± 83 colonies. With the number of colonies on the untreated SUS430 surface taken as 100%, the colony count on the 410-nm LIPSS surface was reduced to approximately 17% (an 83% reduction), while that on the 380-nm/750-nm mixed LIPSS surface was reduced to approximately 69% (a 31% reduction).

These results indicate that narrower ridge and valley widths and higher structural uniformity contribute considerably to the inhibition of bacterial adhesion. These reductions suggest that the surface structures may affect not only initial bacterial adhesion but also subsequent cell viability due to mechanical stresses exerted by the nanostructures.

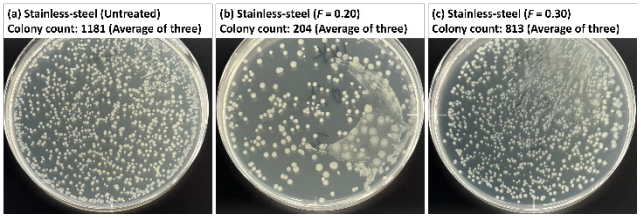

Fig. 6 Images of agar plates showing bacterial colonies: (a) untreated SUS430 surface; (b) 410-nm LIPSS-treated surface; (c) 380-nm/750-nm mixed LIPSS-treated surface.

3.3 Correlation between structural features and antibacterial effect

Table 1 summarizes the relationship between structural parameters (ridge and valley width and structural uniformity) and antibacterial performance. The superior antibacterial performance observed for the 410-nm LIPSS is attributed to both its narrower ridge and valley width and higher structural uniformity. These findings suggest that not only the presence of micro/nano structures but also their precise geometric control plays a critical role in enhancing antibacterial performance. This demonstrates the potential of femtosecond laser processing as an effective approach to impart antibacterial functionality to surfaces without the use of chemical agents.

Furthermore, as schematically illustrated in Fig. 7, considering that bacteria come into direct contact with the LIPSS surface, these nanoscale structures may have imposed physical stress and tension on the bacterial cell membranes and walls. Unlike microscale structures that primarily inhibit colony formation, the nanoscale structures used in this study likely caused direct physical damage to the bacterial surface. Such mechanical interactions are believed to play an important role in the observed antibacterial performance. This mechanical bactericidal mechanism resembles effects reported for natural surfaces such as cicada wings, where nanoscale structures physically rupture bacterial membranes [23].

The potential toxicity of metal ions is widely recognized and cannot be entirely ruled out in this study. However, some studies [24] have evaluated antibacterial performance resulting solely from surface geometry by fabricating micro/nanostructures using non-laser methods and subsequently applying a coating layer to eliminate the influence of the base material. This approach minimizes the influence of the substrate material, allowing evaluation based solely on surface topography. We reason that our experimental results show the structural effect (physical effect) rather than the chemical effect (coming from material toxicity). To clarify the evidence distinguishing these two effects, chemical coating applied on the LIPSS structure as reported in Ref. 24 might be appropriate. To further investigate the antibacterial effect for LIPSS, knowledge of this experimental result is important.

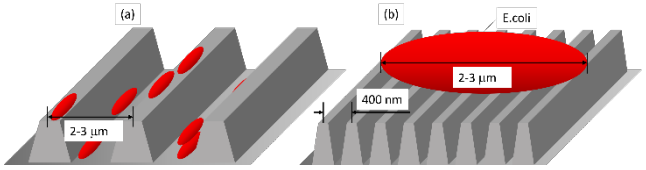

Fig. 7 Schematic illustration showing the interaction between bacteria and surface structures: (a) microscale structures inhibiting colony formation; (b) nanoscale structures inducing physical damage through direct contact.

4. Conclusion

In this study, LIPSS with different ridge and valley widths and uniformities were fabricated on SUS430 stainless-steel surfaces using femtosecond laser processing, and their antibacterial performance was evaluated. Through laser irradiation experiments, LIPSS were successfully formed by vertically irradiating a 1030-nm femtosecond laser onto mirror-polished stainless-steel surfaces. The 410-nm LIPSS structure formed at a fluence of 0.20 J/cm² exhibited narrower ridge and valley widths and higher structural

Table 1 Relationship between structural parameters of LIPSS and antibacterial performance.

Fluence (J/cm^2)	Ridges and valleys (nm)	Structural uniformity (Δω)	Presence of mixed structures	Relative colony count (%)	Inhibition (%)
0.20	~410	0.37	None	17	83
0.30–0.40	~380	0.55–0.81	Mixed (includes ~750 nm)	69	31

uniformity relative to the laser wavelength, resulting in an approximately 83% reduction in *E. coli* colony count. In contrast, the 380-nm/750-nm mixed LIPSS structure formed at 0.30–0.40 J/cm² showed mixed components around 750 nm, lower uniformity, and only about a 31% reduction in colony count. These findings indicate that geometric parameters such as ridge and valley width and structural uniformity play a crucial role in enhancing antibacterial performance.

This study confirms that femtosecond laser processing can impart antibacterial functionality to stainless-steel surfaces without the use of chemical agents, using simple equipment and processes. As laser processing is applicable to a wide range of materials, it enables the post-fabrication functionalization of existing products, distinguishing it from conventional antibacterial approaches. Moreover, since no antibacterial agents are used, this technique offers potential as a countermeasure against antimicrobial-resistant bacteria. Continued research in this area is expected to facilitate future applications in medical devices, food processing, and related fields. Future work will focus on optimizing these structural parameters for different bacterial species and on scaling the fabrication process for industrial applications, particularly in medical devices, food contact surfaces, and public health infrastructure.

Acknowledgments

This research was financially supported by a Grant-in-Aid for Scientific Research (C) (JP16K06745) from the Ministry of Education, Culture, Sports, Science and Technology (MEXT), Japan; the New Energy Industrial Technology Development Organization (NEDO)/Ministry of Economy, Trade and Industry, Japan; the MEXT Quantum Leap Flagship Program (MEXT Q-LEAP) (JPMXS0118070187); the AMADA Foundation (AF-2018203-A3, AF-2022233-B3); the Advanced Analysis Centre in Research Institute of Science and Technology of Tokai University; the Joint Usage/Research Center on Joining and Welding, Osaka University; and Tokai-SPRING SACRA.

References

[1] Ministry of Health, Labour and Welfare (MHLW): "National Action Plan on Antimicrobial Resistance (AMR) 2023–2027", (MHLW, Tokyo, 2023) p.1.
[2] K. K. Chung, J. F. Schumacher, E. M. Sampson, R. A. Burne, P. J. Antonelli, and A. B. Brennan: Biointerphases, 2, (2007) 89.
[3] K. Nakade, K. Jindai, T. Sagawa, H. Kojima, T. Shimizu, S. Shingubara, and T. Ito: ACS Appl. Nano Mater., 1, (2018) 5736.
[4] H. Shimada, K. Watanabe, and M. Yamaguchi: J. Laser Micro Nanoeng., 16, (2021) 94.
[5] R. Takase, S. Kodam, K. Shimada, H. Mescheder, K. Winands, J. Riepe, K. Arntz, M. Mizutani, and T. Kuriyagawa: Int. J. Autom. Technol., 14, (2020) 601.
[6] J. Eichstädt, G. R. B. E. Römer, and A. J. Huis in't Veld: Phys. Procedia, 12, (2011) 7.
[7] Y. Zhang, Y. Jiao, C. Li, C. Chen, J. Li, Y. Hu, D. Wu, and J. Chu: Int. J. Extrem. Manuf., 22, (2020) 032002.
[8] M. Birnbaum: J. Appl. Phys., 36, (1965) 3688.
[9] J. Bonse and J. Krüger, S. Höhm and A. Rosenfeld: J. Laser Appl.,24, (2012) 042006.
[10] R. Buividas, M. Mikutis, and S. Juodkazis: Prog. Quant. Electron., 38, (2014) 119.
[11] M. Okazaki, M. Hashida, and S. Iwamori: J. Laser Appl., 35, (2023) 042075.
[12] K. Schwibbert, A. M. Richter, J. Kruger, and J. Bonse: Laser Photonics Rev., 18, (2024) 2300753.
[13] H. Vaghasiya, and P. T. Miclea: Optics, 4, (2023) 539.
[14] J. Jamdeleit, G. Urbasch, H. D. Hoffmann, H. -G Treush, and E. W. Kreutz: Appl. Phys. A, 63, (1996) 117.
[15] M. Hashida, A. F. Semerok, O. Gobert, G. Petit, Y. Izawa, and J. F- Wagner: Appl. Surf. Sci., 197-198, (2002) 862.
[16] J. Bonse, J.M. Wrobel, K.-W. Brzezinka, N. Esser, and W. Kautek: Appl. Surf. Sci., 202, (2002) 272.
[17] J. Bonse∗, S. Baudach, J. Krüger, W. Kautek, and M. Lenzner: Appl. Phys A, 74, (2002) 19.
[18] K. Takenaka, M. Hashida, H. Sakagami, S. Masuno, M. Kusaba, S. Yamaguchi, S. Iwamori, Y. Sato, and M. Tsukamoto: Rev. Sci. Instrum., 93, (2022) 093001.
[19] B. Wu, M. Zhou, J. Li, X. Ye, G. Li, and L. Cai: Appl. Suf. Sci., 256, (2009) 61.
[20] K. Okamuro, M. Hashida, Y. Miyasaka, Y. Ikuta, S. Tokita, and S. Sakabe: Phys. Rev. B, 82, (2010) 165417.
[21] M. Hashida, Y. Ikuta, Y. Miyasaka, S. Tokita, and S. Sakabe: Appl. Phys. Lett., 102, (2013) 174106.
[22] J. Outon, M. Carbu, M. Dominguez, M. Ramirez-del-Solar, G. Alba, M. Vlahou, E. Stratakis, V. Matres, and E. Blanco: Appl. Surf. Sci., 663, (2024) 160225.
[23] E.P. Ivanova, J. Hasan, H.K. Webb, V.K. Truong, G.S. Watson, J.A. Watson, V.A. Baulin, S. Pogodin, J.Y. Wang, M.J. Tobin, C. Löbbe, and R.J. Crawford: Small, 8, (2012) 2489.
[24] T. Nishitani, K. Saito, H. Ogihara, and T. Ito: J. Surf. Finishing Soc. Jpn., 74, (2023) 412.

(Received: July 3, 2025, Accepted: November 24, 2025)